February 25, 2022

MEMO TO: CARE-74 File

F R O M: Kelly Takaya King, Chair
Climate Action, Resilience, and Environment Committee

SUBJECT: **TRANSMITTAL OF INFORMATIONAL DOCUMENTS RELATING TO BILL 21 (2022), SEABIRD AND BIODIVERSITY PROTECTION** (CARE-74)

The attached informational documents pertain to Item 74 on the Committee's agenda.

care:misc:074afile01:brs

Attachments

The Maui News

Seabird project asks for public's help in stopping fallout incidents

The Maui Nui Seabird Recovery Project is working to protect young seabirds from getting distracted and disoriented from artificial light during what is known as "fallout season."

The Maui News

A conservation group on Maui is working to protect seabirds during *“fallout season,”* a phenomenon that occurs when artificial light from buildings and roadways causes young seabirds to get distracted and disoriented on their first flight to the ocean.

In Hawaii, seabird chicks journey from their burrow nests to the sea for the first time each year from October through December, according to the Maui Nui Seabird Recovery Project, which is typically flooded with calls during this time from concerned people who have found what appears to be a lost or injured seabird.

“These fallout birds can be found in the road, in parking lots, on your lanai, in the park, hiding or in plain sight, and they are in danger,” the organization said in a news release last week. *“Fallout occurs when artificial light from our buildings and roadways causes them to be distracted and disoriented and to fall out or land on the ground instead of in the ocean.”*

Seabird fallout can happen throughout the year with adult seabirds, but it primarily affects fledgling seabirds, mainly the ‘ua’u kani (wedge-tailed shearwaters) and the endangered ‘ua’u and ‘a’o (Hawaiian petrels and Newell’s shearwaters), the organization said.

While making their first flight to the ocean, young seabirds can get lost or injured due to artificial light from buildings and roadways. Maui Nui Seabird Recovery Project photos

Normally, nocturnal instincts, hungry bellies and a strong sense of smell guide seabirds towards the ocean, using natural light from the moon and stars to navigate.

The open ocean is where they spend most of their time living and foraging for food, until they return to land to nest.

"Unfortunately, artificial light at night such as street lights, stadium lights, construction lights, building lights and residential lights are known to distract seabirds from their intended routes," the organization said. *"Artificial lights pose the greatest threat to seabirds and other wildlife when they are unshielded and high in short wavelengths."*

Circling the lights for hours leaves birds tired, dehydrated and more likely to collide with structures or fall to the ground from exhaustion or injury. Once grounded, they are *"extremely vulnerable"* to predators like cats and

ehicle strikes.

Seabirds who suffer from fallout cannot make it to the ocean on their own, which is why locating stranded seabirds and taking steps to rescue them is *"crucial to preserving these native and endangered Hawaiian birds,"* the organization noted.

Residents who find a seabird should carefully place it in a ventilated box with no food or water, then call the Maui Nui Seabird Recovery Project's seabird hotline at (808) 573-BIRD (2473).

Team members will follow up with the individual, meet to collect the seabird, assess its health and collect biological data, band the seabird for long-term tracking and release it out to sea.

"Remember, you can help prevent seabird fallout simply by turning off your lights," the organization said. *"Always use warm temperatures, low in height and fully shielded wildlife-friendly lights. This type of light makes the difference not only for seabirds and other native wildlife but also for stargazing."*

To learn more about lighting ordinances and how light pollution impacts community health, visit mauinuiseabirds.org or darksky.org.

Monthly Notices
of the
ROYAL ASTRONOMICAL SOCIETY

MNRAS **478,** 1776–1783 (2018)
Advance Access publication 2018 May 17

doi:10.1093/mnras/sty1143

Modelling the effects of phosphor converted LED lighting to the night sky of the Haleakala Observatory, Hawaii

M. Aubé,[1]★ A. Simoneau,[2] R. Wainscoat[3] and L. Nelson[2]

[1]*Cégep de Sherbrooke, 475, rue du Cégep, Sherbrooke, Québec J1E 4K1, Canada*
[2]*Bishop's University, 2600 rue College, Sherbrooke, Québec J1M 1Z7, Canada*
[3]*Institute for Astronomy, University of Hawaii, 2680 Woodlawn Dr, Honolulu, HI 96822, USA*

Accepted 2018 April 28. Received 2018 April 27; in original form 2018 February 27

ABSTRACT

The goal of this study is to evaluate the current level of light pollution in the night sky at the Haleakala Observatory on the island of Maui in Hawaii. This is accomplished with a numerical model that was tested in the first International Dark Sky Reserve located in Mont-Mégantic National Park in Canada. The model uses ground data on the artificial light sources present in the region of study, geographical data, and remotely sensed data for (1) The nightly upward radiance, (2) The terrain elevation, and 3) The ground spectral reflectance of the region. The results of the model give a measure of the current state of the sky spectral radiance at the Haleakala Observatory. Then, using the current state as a reference point, multiple light conversion plans are elaborated and evaluated using the model. We can thus estimate the expected impact of each conversion plan on the night sky radiance spectrum. A complete conversion to white light emitting diodes (LEDs) with correlated colour temperature of 4000 and 3000 K are contrasted with a conversion using phosphore-convertred amber LEDs. We include recommendations concerning the street lamps to be used in sensitive areas like the cities of Kahului and Kihei, and suggest best lighting practices related to the colour of lamps used at night.

Key words: radiative transfer – light polution.

1 INTRODUCTION

The evaluation of the night sky spectral radiance under clear conditions is a complex task given the large number of dependant variables. Indeed, Aubé (2015) showed that the sky radiance is a non-trivial function of the aerosol and molecular atmospheric content along with the geographical distribution of anthropogenic light sources on the ground and their relationship with the nearby optical and geometrical properties like the underlying ground spectral reflectance, the topography, and the presence of small to medium size blocking obstacles (e.g. trees and buildings). Many factors are variable with time like ground reflectance, tree foliage, aerosol concentration and composition profiles, sports lighting, ornamental lights, and car headlights. The large variance in some of the key variables has been noted by many authors (Dobler et al. 2015; Meier 2018), and this results in a large variance in the inferred sky brightness data (Aubé 2007; Patat 2008; Falchi 2011; Pun & So 2012; Aubé et al. 2014; Puschnig, Posch & Uttenthaler 2014; Pun et al. 2014; Kyba et al. 2015; Sánchez de Miguel 2015; Sánchez de Miguel et al. 2017). This variation in the driving variables makes it difficult to identify the origin of the sky radiance fluctuations because one should record at the same time many other quantities such as the aerosol optical depth (AOD) and Angstrom coefficient α (or the concentration, chemical composition, and size distribution of aerosols). Another factor affecting observations is that low-altitude clouds below the observer sometimes block and suppress artificial light from ground based sources (Pedani 2004; Ribas et al. 2016). Our analysis assumes the more common case of clear sky without low-altitude clouds.

One other way to evaluate the evolution of the sky radiance is the use of a radiative transfer model that allows the selection of diverse values of the key variables identified above, hence allowing them to be maintained at some predefined fixed values. Many night sky brightness models have been constructed since the 1980s. Some are based on homogeneous or simplistic geographical descriptions of the key variables like the Garstang model (Garstang 1986). According to this paper, a city can be modelled as a perfect circle of constant ground level light flux, ground reflectance, and angular emission function. Moreover, the topography is flat and the second-order of scattering is not explicitly calculated. Some improvements of the Garstang model have been proposed (Luginbuhl et al. 2009; Cinzano & Falchi 2012) to minimize these limitations. Recent models take account of the complexity of the environment and hence

★ E-mail: martin.aube@cegepsherbrooke.qc.ca

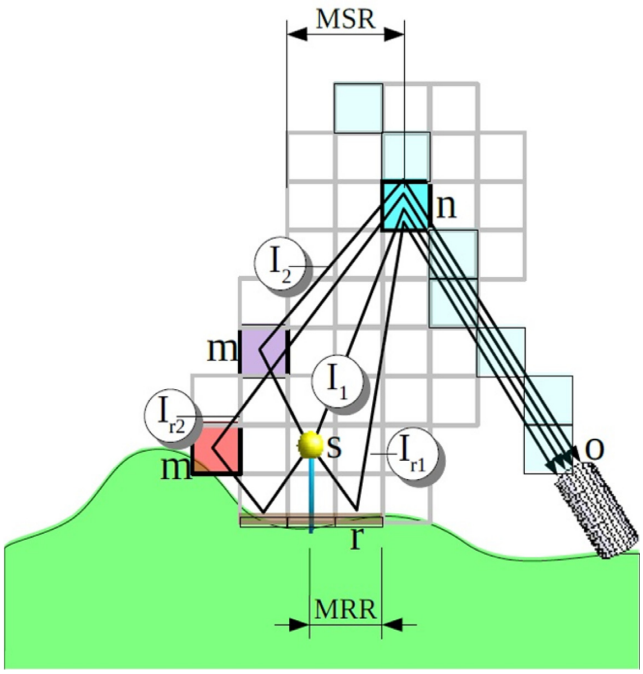

Figure 1. Optical path considered in the calculation of the artificial sky radiance in the Illumina model. 'o' is the virtual observer, 'n' a voxel in the line of sight, 's' a cell containing a light source, 'm' are voxels where second-order scattering occurs, and 'r' is a voxel where light reflects off the ground. 'MRR' is the maximal reflection radius, the distance within which light can reflect off the ground, and 'MSR' is the maximal scattering radius, the distance within which second-order scattering is being considered (Aubé 2007).

are more realistic with regards to real situations (Baddiley 2007; Kocifaj 2007; Luginbuhl et al. 2009; Cinzano & Falchi 2012; Aubé 2015; Falchi et al. 2016; Aubé & Simoneau 2018).

2 DATA

The model used in this study is called Illumina (Aubé et al. 2005; Aubé 2015; Aubé & Simoneau 2018). The model simulates the reading of a virtual spectrometer by using ray-tracing techniques along with statistical selection of tracing photons. A virtual instrument or observer is located on the voxel based simulation domain characterized by a radiant flux map of the light sources on the territory, by the angular photometry and spectral power distribution (SPD) of these light sources, and by a description of the environment's physical properties. The position and direction of observation of the observer defines a line of sight along which any scattered light can propagate towards the virtual instrument and hence be detected. The model calculates a statistically selected set of possible optical paths from the light sources in the domain to every point on the line of sight, taking into account multiple scatterings and reflections along the way *(See Fig. 1)*. By adding the contribution of every optical path, the total artificial sky brightness is obtained.

Some assumptions are made to facilitate the calculations. Due to the fact that a cell covers an area of one square kilometre, the variations in the angular light output pattern (LOP) with the azimuthal angle are neglected since an area of this size is expected to contain many light sources and that their orientation can vary greatly depending on the way the streets are designed. To the best

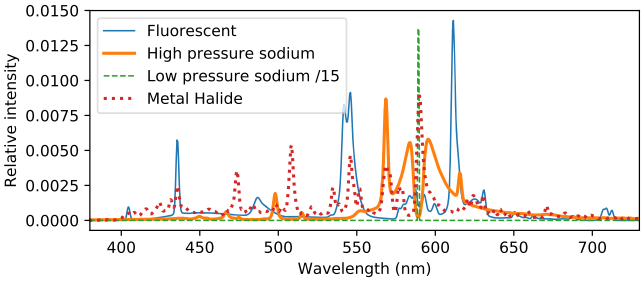

Figure 2. Photopic normalized spectra of high-intensity discharge lamps. The LPS spectrum has been reduced by a factor 15 for scale.

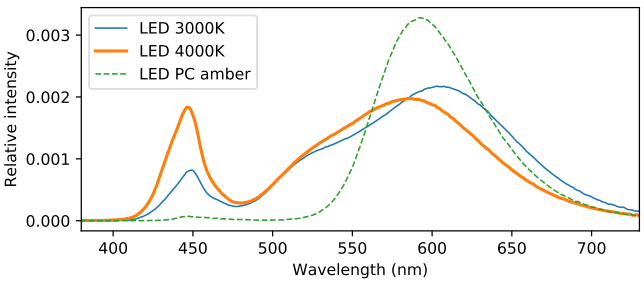

Figure 3. Photopic normalized spectra of LED lamps.

of our knowledge, an in-dept analysis of the validity of that assumption has not yet been made. Based on some estimates made prior to the model design, only four kinds of optical paths are worth considering when trying to attain a ≈1 per cent precision. Actually, Aubé (2015) showed that for low aerosol loadings (AOD ≈ 0.1), the contribution of the second-order of scattering is generally lower inside the city perimeter (≈7 per cent), but this percentage increases rapidly when exiting the city. The maximum contribution of the second-order of scattering is obtained near the city limit, where it can reach 38 per cent without the blocking effect generated by obstacles. Previous modelling experiments we conducted showed that for moderate distance to the source (<30 km) the contribution of the third order of scattering is lower than 1 per cent of the total. This result is confirmed by Kocifaj (2018a) who stated that higher order of scattering are negligible up to 30 km from the source for blue light and up to 60 km for red light. Since our main light sources are located within 30 km of the observatory, we can neglect higher scattering orders. For that reason, only first and second-order scattering with and without a reflection from the ground underneath the light source are computed.

The basic SPDs used in this study are presented in Figs 2 and 3. The base LOPs are presented in Fig. 4.

2.1 Modelling domain characteristics

The domain is a 500 x 400 km rectangle centred on (20.306N, 156.442W) in the spatial reference system NAD83(HARN)/UTM zone 04N (EPSG:3750). This envelopes most of the Hawaii archipelago, with the exclusion of Kauai island. The virtual observer is located at the Haleakala observatory on the Island of Maui (20.708N, 156.257W) looking at 20° of elevation and with an azimuthal angle of 292°. This is actually pointing towards Honolulu.

Fig. 5 shows the terrain visible by an observer located 20 ft above the Haleakala observatory in direct line of sight, meaning that it is not blocked by the topography. To produce the maps we took into

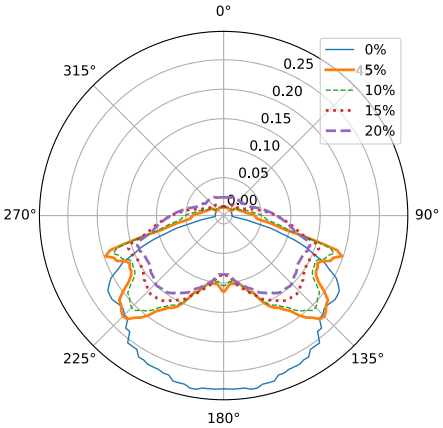

Figure 4. LOPs used by the model. The percentage represents the ULOR of the lamp.

account the Earth's curvature. One can see that most of Honolulu is in the shadow. The main cities on Big Island are also completely in the shadow. However, closer to the observatory on Maui island, both the cities of Kihei and Kahului are in the direct line of sight, with Kahului being the most illuminated. Both cities are near the observatory within a distance of 30 km.

In those cities, most buildings are single story structures with few trees. All of this makes it so that the public light sources are typically above everything else, with very few obstacles blocking the light from directly escaping the city.

The average obstacle height, distance, and filling factor as well as the average height of the light sources were estimated by random sampling and are shown in Table 1. We mostly focused on the brightest city, Honolulu, and the closest one, Kahului. The sampling was done using Google Earth to estimate the obstacles separation and Google StreetView for the rest. These parameters were chosen to be uniform throughout the territory due to the small variation observed in the city of Kahului and the fact that this city is the main source of light pollution, as can be inferred from Fig. 5.

The filling factor of the obstacles is the opacity of the obstacles to light, that is to say the ratio of the light rays that can pass through or between the obstacles. A better approach would be the one described by Kocifaj (2018b), where one takes into account multiple rows of buildings instead of a single one in addition to various other improvements. This may be included in our model in the future. The value 0.5 was estimated using Google StreetView, while considering mainly Kahului for the reasons mentioned above. Second-order scattering was calculated whitin 4 km of the main optical path (MSR in Fig. 1).

2.2 Estimation of the Hawaii lighting infrastructure

Many parameters were estimated for different circular regions of the modelling domain (see Fig. 6). When two or more regions overlap, the one with the higher index takes precedence. Each region was defined assuming a relative uniformity of their lamps and obstacles characteristics. Table 1 contains the lamps and obstacle characteristics for each region. To estimate the mean lamp and obstacle heights, we used the 3D model available on Google Earth as well as the views from Google StreetView. We estimated the lamps upward light output ratio (ULOR) and SPD according to our knowledge of the islands' lighting infrastructure.

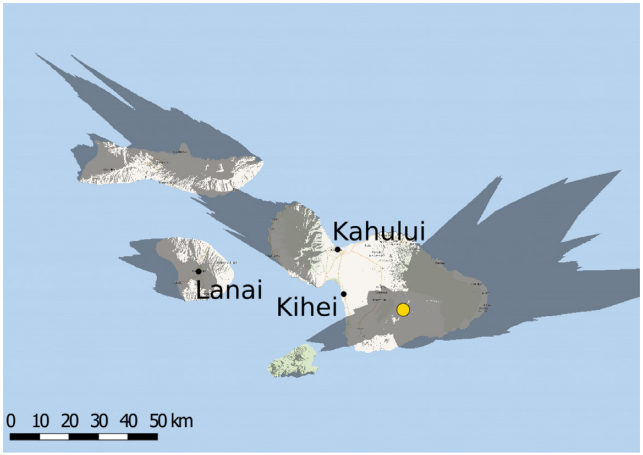

(a)

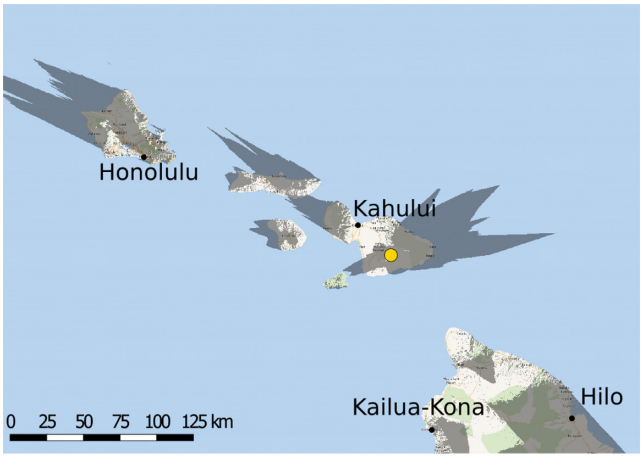

(b)

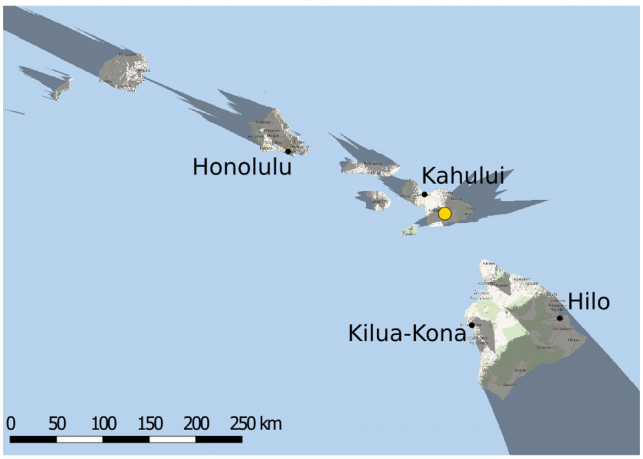

(c)

Figure 5. Viewshed from the Haleakala Observatory. The shaded regions correspond to regions that are not visible in the direct line of sight from 20 ft (approx. 6.1 m) above the observatory (yellow dot). *Determined using data from heywhatsthat.com.*

2.3 Other input data and modelling parameters

The ground reflectance is obtained from the Moderate Resolution Imaging Spectroradiometer (MODIS) MYD09A1 data set (Kaufman & Tanré 1998) for the period ranging from 2014 May 17 to

Table 1. Lighting infrastructure and obstacle characteristics estimated with Google StreetView. Cobraheads are characterized with 5 per cent ULOR, athletic facilities to 10 per cent ULOR, and full shielding to 0 per cent ULOR. 'Per cent' represent the relative amount (in per cents) of the light from the region that is coming from the associated characteristics. The technology used are low-pressure sodium (LPS), high-pressure sodium (HPS), metal hallide (MH), and compact uorescent lamps (CFLs).

#	Zone	Per cent	Technology	Shielding	Lamp height	Obstacle height	Obstacle distance	Obstacle filling factor
1.	Oahu	90%	HPS	Cobrahead	7 m	5 m	25 m	0.5
		10%	MH	Athletic facilities				
2.	MCBH	35%	CFL	5% ULOR	7 m	5 m	25 m	0.5
		65%	HPS	20% ULOR				
3.	Kailua	50%	LPS	10% ULOR	7 m	5 m	25 m	0.5
		40%	HPS	Cobrahead				
		10%	MH	Athletic facilities				
4.	Honolulu port	100%	HPS	10% ULOR	7 m	5 m	25 m	0.5
5.	Airport /	70%	HPS	10% ULOR	7 m	5 m	25 m	0.5
	Hickam AFB	30%	MH	10% ULOR				
6.	Industrial area	80%	HPS	20% ULOR	7 m	5 m	25 m	0.5
		20%	MH	20% ULOR				
7.	Kahala	50%	LPS	10% ULOR	7 m	5 m	25 m	0.5
		40%	HPS	Cobrahead				
		10%	MH	Athletic facilities				
8.	Waipahu	50%	LPS	10% ULOR	7 m	5 m	25 m	0.5
		40%	HPS	Cobrahead				
		10%	MH	Athletic facilities				
9.	Mililani	50%	LPS	10% ULOR	7 m	5 m	25 m	0.5
		40%	HPS	Cobrahead				
		10%	MH	Athletic facilities				
10.	Waikiki	40%	HPS	Fully shielded	7 m	5 m	25 m	0.5
		40%	HPS	10% ULOR				
		20%	MH	20% ULOR				
11.	Molokai	90%	HPS	Cobrahead	7 m	5 m	25 m	0.5
	and Lanai	10%	MH	10% ULOR				
12.	Molokai airport	100%	HPS	15% ULOR	7 m	5 m	25 m	0.5
13.	Lanai airport	100%	HPS	15% ULOR	7 m	5 m	25 m	0.5
14.	Maui	72%	HPS	Fully shielded	7 m	5 m	25 m	0.5
		18%	HPS	10% ULOR				
		10%	MH	10% ULOR				
15.	Kahului airport	95%	HPS	10% ULOR	7 m	5 m	25 m	0.5
	and port	5%	MH	10% ULOR				
16.	Big Island	87%	LPS	10% ULOR	7 m	5 m	25 m	0.5
		8%	HPS	10% ULOR				
		5%	MH	5% ULOR				
17.	Lava lakes	– %	—	Volcano lava	– m	– m	– m	—
18.	Hilo	70%	LPS	10% ULOR	7 m	5 m	25 m	0.5
		30%	HPS	15% ULOR				
19.	Kona airport	85%	HPS	10% ULOR	7 m	5 m	25 m	0.5
		10%	LPS	10% ULOR				
		5%	MH	20% ULOR				
20.	Kona	70%	LPS	10% ULOR	7 m	5 m	25 m	0.5
		20%	HPS	15% ULOR				
		10%	MH	15% ULOR				

May 24, which has a resolution of 500 m but was resampled to 1 km, and is presented at Fig. 7. The digital elevation model used comes from the Shuttle Radar Topography Mission (SRTM) data (Farr et al. 2007) and is presented in Fig. 8 which has a native horizontal resolution of 3 arcsec (about 90 m) but is also being resampled to 1 km. The radiant flux map is derived using steps presented in Aubé & Simoneau (2017) using satellite imagery at night from the visible infrared imaging radiometer suite day/night band (VIIRS-DNB) VCMSLCFG data set (Elvidge et al. 2017) for the month of 2014 May resampled to 1 km from the original 15 arcsec presented in Fig. 9. Our estimate of the lighting infrastructure consider all light detected with VIIRS being emitted either by sport fields or by streetlights but we know that a substantial part of it is coming from other sources like outdoor private lighting, buildings windows, and car headlights. A number of studies aimed to estimate the relative contribution of the streetlight to the total artificial light at night. Streetlights contribution was estimated to lie between 30 per cent and 50 per cent of the total artificial light at night (Lockwood, Thompson & Floyd 1990; Hiscocks & Gudmundsson 2010; Kuechly et al. 2012). The absolute values that we obtain with the model are certainly overestimated but we do not know the actual percentage of light coming exclusively from streetlights in Hawaii. This should not be an important issue when we are looking to ratios between scenarios but it is certainly a problem for the absolute values (e.g. Fig. 10). In the latter case, one must consider the values as more or less proportional to what would be observed with

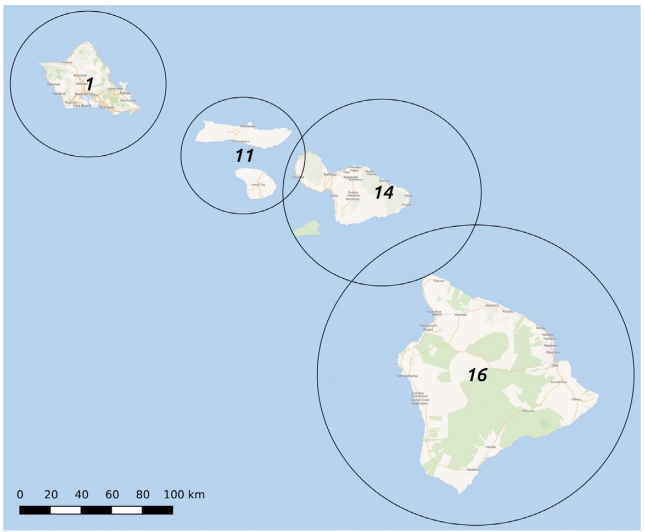

(a) Main islands

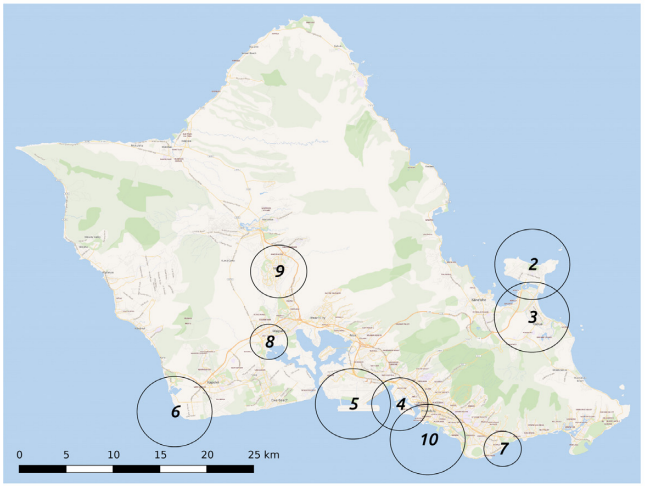

(b) Oahu

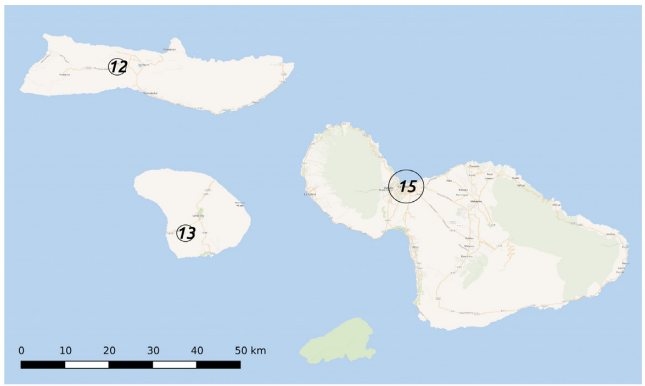

(c) Maui, Lanai and Molokai

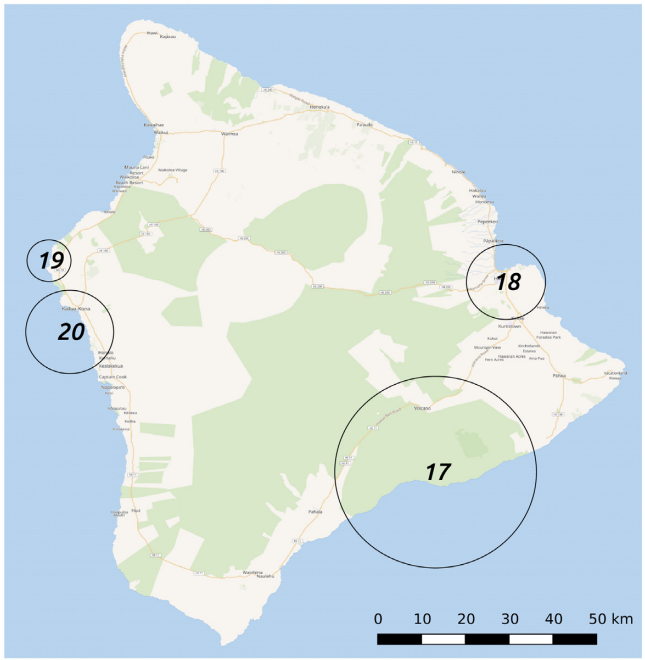

(d) Big Island

Figure 6. Approximative zones used for the simulation. In case of overlap, the zone with the higher index takes precedence.

Table 2. Atmospheric parameter used, based on data from Holben et al. (2001). τ_a is for a reference wavelength of 500 nm while α is derived from AERONET bands 440, 500, 675, and 870 nm.

P_0	α	τ_α	R_H	Aerosol type
101.3 kPa	0.70	0.11	70	Maritime

P_0 : ground air pressure.
α : Angstrom exponent.
τ_α : aerosol optical depth.
R_H : relative humidity.

only streetlights and sports fields on. Another caveat is that we do not know anything about the spectral and angular characteristics of other lighting but streetlights.

Eventually, the model will be able to make use of data from VIIRS-DNB for the intensity of the light sources but also use data from the International Space Station to evaluate the SPD of the sources (Sánchez de Miguel 2015) and the approach developed by Kocifaj (2018b) to find the net emission function. In that way we will be able to fully take into account all the

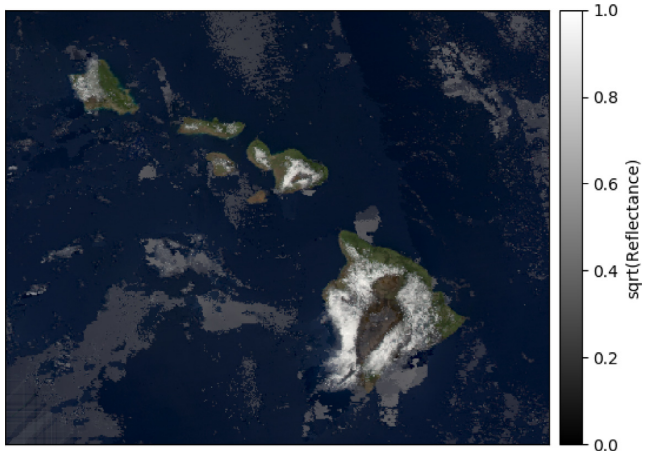

Figure 7. MODIS MYD09A1 RGB composite imagery for the month of 2014 May. [*R = band 1 (645 nm), G = band 4 (555 nm) and B = band 3 (469 nm)]* Each band fluctuates between 0 and 1.

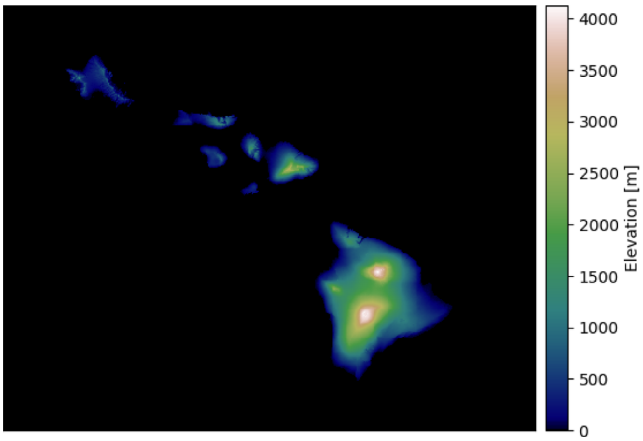

Figure 8. SRTM data.

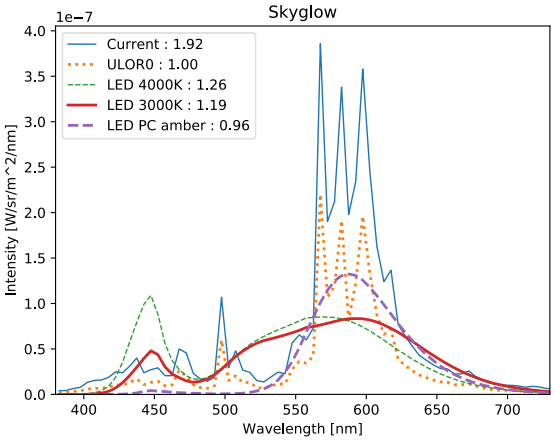

(a) Raw skyglow

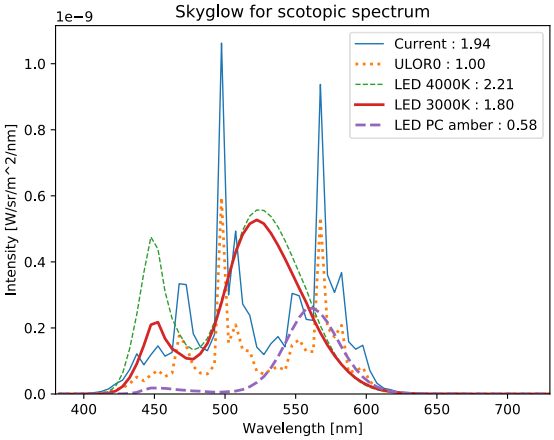

(b) Scotopic skyglow

Figure 9. VIIRS-DNB data (logscale).

light sources present in the domain and not restrict ourselves to streetlights.

The AOD or τ_a and Angstrom exponent α shown in Table 2 come from Holben et al. (2001), whose climatology is based on the average of the Aerosol Robotic Network (AERONET) (Holben et al. 1998) data for 38 clear days in May between the years 1995

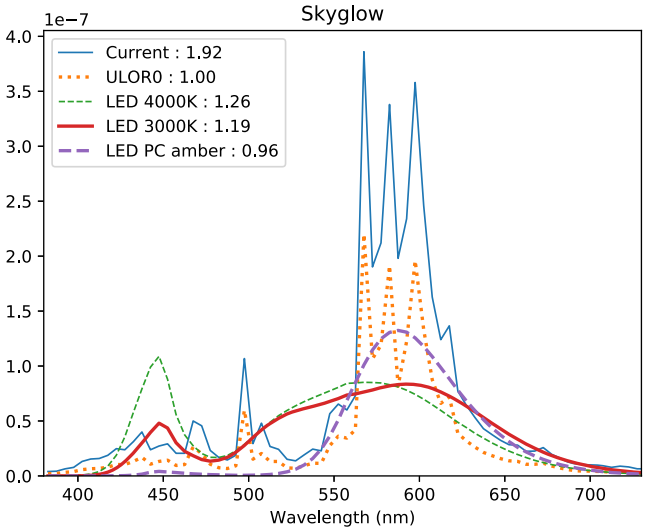

(a) Raw skyglow

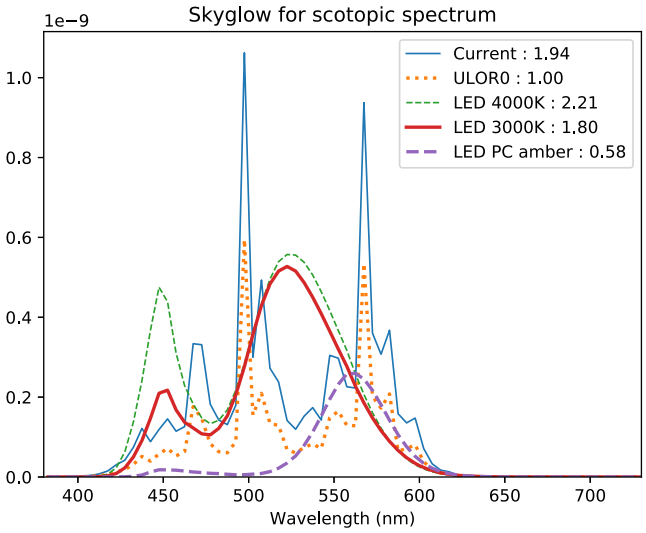

(b) Scotopic skyglow

Figure 10. Sky radiance spectra (a) for different lighting scenarios and its skyglow impact on the scotopic vision (b). The numbers given in the legend of each panel are equal to the ratio of the integral of the associated curve to the integral of 'ULOR0'. Panel 10a is the raw spectra without any weighting and is the most useful one for professional astronomy.

and 1999 for the site of Lanai, HI. The AOD is for a reference wavelength $\lambda_0 = 500$nm while α is derived from AERONET bands 440, 500, 675, and 870 nm using a linear regression. The AOD values for other wavelengths are extrapolated from theses values and Mie's power law, where

$$\frac{\tau_\lambda}{\tau_{\lambda_0}} = \left(\frac{\lambda}{\lambda_0}\right)^{-\alpha} \quad . \tag{1}$$

3 RESULTS AND DISCUSSION

The model was run for ninety 5 nm-wide spectral bands equally spaced between 380 and 830 nm. The model output for different lighting scenarios, namely 'Current', representing the most accurate

estimate of the current situation on the archipelago, 'ULOR0' being the same spectral mix as the current scenario but with every lamp head replaced by a full cut-off (0 per cent ULOR). This allows us to isolate the effect of the uplight on the sky radiance spectrum. Then 'LED 4000 K', 'LED 3000 K', and 'LED PC amber' are estimated with a full conversion to these respective technologies with full cut-off heads while keeping the installed lamp's luminous flux constant. The reference spectra are shown in Figs 2 and 3, while the LOPs are shown in Fig. 4.

The model also outputs a map of the contribution of the lights sources to the sky radiance, which can be integrated over the zones described in Figure 6. We obtain a scotopic weighted contribution of 2.1 per cent for Ohau, 1.1 per cent for Molokai and Lanai, 96.3 per cent for Maui and 0.3 per cent for Big Island. This shows that Kahului, the main city of the island of Maui, is the main source of the light seen at the observatory and that Honolulu can be neglected when considering the impact of conversion plans.

Fig. 10 shows the spectral radiance data obtained for the different simulated scenarios. It also shows the spectra when weighted by the nighttime vision (scotopic) sensitivity curve (Wyszecki & Stiles 1982). Please note that any conclusion drawn from Fig. 10 is only valid for this particular site, where the most contributing source, Kahului, has obstacles that are lower than the light sources and is in direct line of sight of the observatory. Note also that obstacles characteristics where chosen to be uniform over the whole territory because other important light sources are relatively far away and have a negligible contribution. A more precise description should include a more detailed definition of the subgrid obstacles. Other configurations, especially when obstacles are higher than light fixtures for nearby sources, may lead to very different results and thus new modelling procedures should be implemented.

By looking at Fig. 10(a), which is the most interesting one for professional astronomy since it is not weighted by the scotopic sensitivity, the impact of reduced uplight is obvious. This is especially clear for the current and current w/o uplight curves, where we can see that removing the uplight while keeping the same luminous flux reduces the sky radiance by an average factor of $\approx$2. On that figure, the numbers indicated in the legends represent the spectral integration reported to the value of the current mix of lamps spectra but without uplight while keeping the same flux (ULOR0.) Both 3000 and 4000 K LEDs produce an averaged radiance greater than ULOR0 indicating that both 4000 and 3000 K LEDs produce a higher level of sky radiance when not considering the change in uplight and keeping the same luminous flux.

The scotopic brightness however, presented in Fig. 10(b), shows clearly the impact of the colour temperature of the LED on the perceived radiance as seen by the dark adapted human eye. Both 4000 and 3000 K LEDs have an average scotopic weighted impact relatively close to the current situation (inside 14 per cent of deviation). Meaning that the brightness reduction provided by the absence of upward light emission for the LEDs is compensated by scotopic brightness associated to the blue content of LEDs. On the other hand, the scotopic brightness generated by PC amber LEDs, is about one third of the scotopic brightness of the current situation. This is due to their low blue light content and their absence of upward light emission. 4000 and 3000 K LEDs have an average scotopic weighted impact about twice the ULOR0 scenario.

The night sky in the 400–550 nm region of the spectrum (blue-green) is naturally extremely dark when the moon is down, or only a thin crescent is illuminated. This is a precious region of the sky for astronomy, and is almost untouched by sodium light sources. At 555 nm, there is a bright yellow-green oxygen line, and astronomers have designed a filter system that avoids this line (with the *g* filter encompassing the blue-green colours short of this wavelength, and the *r* filter encompassing the yellow-red visible light to the red). To the red from 555 nm, are natural sodium and oxygen atmospheric emission lines. The night sky is naturally brighter in the yellow-red wavelengths than in the blue-green wavelengths. Conversion to white LED lighting inevitably moves artificial light into the blue-green part of the spectrum. Use of Amber LEDs greatly minimizes damage to the naturally dark blue-green region of the spectrum. Filtered LEDs, where a filter removes blue LED light emission (such as those in use on the Island of Hawaii), are another alternative to white LEDs that lessen damage to the blue-green part of the night sky spectrum.

4 CONCLUSIONS

The results of this study show that sky radiance for the site of Halaekala observatory in the particular observation direction of 20° of elevation and with an azimuthal angle of 292° (towards Honolulu) is highly sensitive to uplight, largely due to the direct line of sight between the observatory and some nearby cities. For the raw/astronomical impact as well as for the scotopic weighted skyglow, removing the uplight reduces the impact by a factor of approximately two. The county lighting ordinance already requires that all lights are fully shielded, but there remain many cases of unshielded lights. Sports lighting is exempted from this shielding requirements and is particularly damaging.

Because of the effect of the uplight, the current scenario (HPS and MH mix with uplight) produces an impact similar to 4000 and 3000 K LEDs, when looking at the averaged scotopic impact. It can also be seen that the colour temperature for LED lighting has a huge influence on the observed sky radiance, with 4000 K LEDs producing a scotopic brightness nearly four times greater than that for PC amber LEDs. Even 3000 K LEDs produce a scotopic brightness that is three times greater than the PC amber when the conversion is made at constant (installed) luminous flux. Any scenario of LED installation without complete elimination of unshielded lights will result in degradation of the sky brightness.

Although skyglow seems to be very sensitive to uplight, it is important to remember that this is due to the particular geography and cityscape of the region (no blocking by terrain towards nearby cities and obstacles lower than lamps). But when there is no upward light emission, both 4000 and 3000 K LEDs produce skyglow greater than the ULOR0 scenario, which is mainly high-pressure sodium and a few metal halide lamps. The PC amber LEDs, however, produce significatively less skyglow than every other technology tested. For that reason, PC amber LEDs should always be preferred over 3000 and 4000 K LEDs when considering light conversion plans which aim to restrict the sky brightness.

However, one needs to take into account that when such a conversion to LEDs occurs, the luminous flux is often reduced by 30–50 per cent because of the better concentration of the light on the street surface that can generally be achieved with LEDs (Kinzey et al. 2017). In such cases the impacts shown in the previous figures need to be multiplied by a factor 0.5–0.7. But since this reduction is only caused by better optics and not by a better luminous efficiency of LEDs, it would, in principle, be possible to develop HPS lamps with good optics that would produce the same flux reduction because of a better concentration of the light. This is due to the fact that lighting professionals generally want to keep the same illuminance level on the ground while reducing the total luminous flux. It is, however, true that the design of such optics is far easier with

LEDs due to their relative size. LED can also be operated efficiently at low power. But these benefits are true for all LEDs, including PC amber LEDs. Therefore, this is not an argument to favour 4000 and 3000 K LEDs lights.

Lower CCT LEDs, such as 2700 K, are now becoming more common. These were not discussed in detail in this paper, but their impact on astronomy can be inferred by interpolation between the cases on 3000 K and PC amber. In cases where white light is necessary, 2700 K (or lower CCT) should always be chosen over higher CCT LEDs. In cases where white light is not necessary, PC amber LEDs should be used; LEDs that are filtered to remove blue light may also be considered.

ACKNOWLEDGEMENTS

We applied the sequence-determines-credit approach (Tscharntke et al. 2007) for the sequence of authors. Some computations were carried out on the Mammouth Serial II cluster managed by Calcul Québec and Compute Canada. The operation of these supercomputers is funded by the Canada Foundation for Innovation (CFI), NanoQuébec, Réseau de Médecine Génétique Appliquée, and the Fonds de recherche du Québec – Nature et technologies (FRQNT). MA thanks the FQRNT for financial support through the Research program for college researchers . AS thanks the Centre de Recherche d'Astrophysique du Quebec (CRAQ) and FRQNT for financial support. LN thanks the Natural Sciences and Engineering Research Council (Canada) for financial support through the Discovery Grants program.

REFERENCES

Aubé M., Proceedings of Starlight 2007 conference, La Palma, Spain, 2007
Aubé M., 2015, Phil. Trans. R. Soc. B, 370
Aubé M., Simoneau A., 2018, J. Quant. Spectrosc. Radiat. Transfer, 211, 25
Aubé M., Franchomme-Fossé L., Robert-Staehler P., Houle V., 2005, Proc.SPIE, San Diego, California, US, 5890, p. 589012
Aubé M., Fortin N., Turcotte S., García B., Mancilla A., Maya J., 2014, PASP, 126, 1068
Aubé M., Simoneau A. 2017, Illumina Users Guide, available at: http://cegepsherbrooke.qc.ca/~aubema/index.php/Prof/IlluminaGuide2016
Baddiley C., 2007, Starlight: A Common Heritage, La Palma, Spain
Cinzano P., Falchi F., 2012, MNRAS, 427, 3337
Dobler G. et al., 2015, Inf. Syst., 54, 115
Elvidge C. D., Baugh K., Zhizhin M., Hsu F. C., Ghosh T., 2017, Int. J. Remote Sens., 38, 5860
Falchi F., 2011, MNRAS, 412, 33
Falchi F. et al., 2016, Sci. Adv., 2
Farr T. G. et al., 2007, Rev. Geophys., 45
Garstang R., 1986, PASP, 98, 364
Hiscocks P. D., Gudmundsson S., 2010, J. R. Astron. Soc. Can., 104, 190
Holben B. N. et al., 1998, Remote Sens. Environ., 66, 1
Holben B. et al., 2001, J. Geophys. Res.: Atmos., 106, 12067
Kaufman Y. J., Tanré D., 1998, NASA MODIS Algorithm Theoretical Basis Document, Vol. 85, Goddard Space Flight Center, p. 3
Kinzey B., Perrin T. E., Miller N. J., Kocifaj M., Aubé M., Lamphar H. S., Carlson T., 2017, US Depatment of Energy, US
Kocifaj M., 2007, Appl. Opt., 46, 3013
Kocifaj M., 2018a, J. Quant. Spectrosc. Radiat. Transfer, 206, 260
Kocifaj M., 2018b, J. Quant. Spectrosc. Radiat. Transfer, 205, 253
Kuechly H. U., Kyba C. C., Ruhtz T., Lindemann C., Wolter C., Fischer J., Hölker F., 2012, Remote Sens. Environ., 126, 39
Kyba C. C. et al., 2015, Sci. Rep., 5
Lockwood G., Thompson D., Floyd R., 1990, PASP, 102, 481
Luginbuhl C. B., Duriscoe D. M., Moore C. W., Richman A., Lockwood G. W., Davis D. R., 2009, PASP, 121, 204
Meier J. M., 2018, Int. J. Sustainable Light., 19, 142
Patat F., 2008, A&A, 481, 575
Pedani M., 2004, New Astron., 9, 641
Pun C. S. J., So C. W., 2012, Environ. Monit. Assess., 184, 2537
Pun C. S. J., So C. W., Leung W. Y., Wong C. F., 2014, J. Quant. Spectrosc. Radiat. Transfer, 139, 90
Puschnig J., Posch T., Uttenthaler S., 2014, J. Quant. Spectrosc. Radiat. Transfer, 139, 64
Ribas S. J., Torra J., Paricio S., Canal-Domingo R., 2016, Int. J. Sustainable Light., 18, 32
Sánchez de Miguel A., 2015, PhD thesis, Univ. Complutense de Madrid
Sánchez de Miguel A., Aubé M., Zamorano J., Kocifaj M., Roby J., Tapia C., 2017, MNRAS, 467, 2966
Tscharntke T., Hochberg M. E., Rand T. A., Resh V. H., Krauss J., 2007, PLoS Biol., 5, e18
Wyszecki G., Stiles W. S., 1982, Colour Science Vol. 8. Wiley, New York

This paper has been typeset from a TEX/LATEX file prepared by the author.